Friction **12**(11): 2576–2593 (2024)
https://doi.org/10.1007/s40544-024-0922-3
ISSN 2223-7690
CN 10-1237/TH

RESEARCH ARTICLE

Pin-on-disc tribological characterization of single ingredients used in a brake pad friction material

Davide CARLEVARIS[1,*], **Francesco VARRIALE**[2,3], **Jens WAHLSTRÖM**[3], **Cinzia MENAPACE**[1]

[1] *Department of Industrial Engineering, University of Trento, Trento 38123, Italy*

[2] *Brembo S.p.A, Stezzano, Bergamo 24040, Italy*

[3] *Department of Mechanical Engineering Sciences, Lund University, Lund 22100, Sweden*

Received: 11 January 2024 / Revised: 25 March 2024 / Accepted: 20 April 2024

Abstract: Researchers have long been studying the effects of the modification of friction material compositions on their tribological properties. Predictive models have also been developed, but they are of limited use in the design of new compositions. Therefore, this research aims to investigate the tribological behaviour of single ingredients in friction materials to develop a tribological dataset. This dataset could then be used as a foundation for a cellular automaton (CA) predictive model, intended to be a tool for designing friction materials. Tribological samples were almost entirely composed of four distinct friction material ingredients, and one sample composed of their mixture was successfully produced. Pin-on-disc (PoD) tribometer testing and scanning electron microscopy/energy-dispersive X-ray spectroscopy (SEM/EDXS) analysis were used for the tribological characterization. Each material showed distinct tribological properties and evolution of the contact surface features, and the synergistic effect of their mutual interaction was also demonstrated by their mixture.

Keywords: disc brakes; sliding contact; wear behaviour; scanning electron microscopy (SEM); modelling

1 Introduction

Pin-on-disc (PoD) tribometer tests are largely used to investigate the tribological properties of several materials, allowing for the analysis of the wear mechanisms occurring in the sliding contact between a pin and a counterpart, which is generally constituted by a rotating disc. These tests are commonly carried out to investigate the relationship between the tribological properties of the contact interface and parameters such as contact pressure (P_C), sliding velocity, and temperature. Some analyses are performed for railway applications [1, 2], but most PoD experimental tests are conducted to investigate the tribological properties and the airborne particle emissions of automotive brake systems [3–8]. The latter are increasingly gaining interest from the industry and the competent authorities, especially with introducing Euro 7 regulations about non-exhaust emissions [9].

Friction pads for automotive applications are mainly composed of four different material families, i.e., binder, reinforcing fibers, fillers, and friction modifiers [10], for more than 35 ingredients constituting the final compound. A change in one of them with another type of material, or a variation in its percentage in the mixture formulation, results in entirely different tribological properties of the brake pad in terms of coefficient of friction (COF) and wear [11–13]. Several studies were conducted investigating the influence of a single material on tribological properties by substituting, adding, or subtracting one ingredient in the mixture [12, 14–21]. Kumar and Bijwe [14] produced four distinct friction material samples, each containing 10 wt% of a different metal component. These samples underwent experimental testing using

* Corresponding author: Davide CARLEVARIS, E-mail: davide.carlevaris@unitn.it

Abbreviations

AF	Aramid fiber	K_a	Specific wear coefficient
BSE	Backscattered electrons	Ph	Phenolic resin
CA	Cellular automaton	PoD	Pin-on-disc tribometer
COF	Coefficient of friction	SEM	Scanning electron microscope
EDXS	Energy-dispersive X-ray spectroscopy	SF	Steel fiber
FEM	Finite element method	μ	Coefficient of friction
Gr	Graphite		

a reduced-scale semi-component Krauss type test rig. The same authors investigated the role of copper particle morphology by substituting $BaSO_4$ filler in a friction material composition [15]. Cho et al. [16] delved into the impact of three distinct solid lubricants, altering the proportions of graphite (Gr), Sb_2S_3, and MoS_2 within a friction material composition and subjecting them to brake dynamometer testing. Zheng et al. [17] added various proportions of Fe and Gr to friction materials to study their effect on friction and wear properties. Mahale et al. [18] studied the effect of different potassium-titanate granulometry as additions to NAO brake pad compositions. Many authors have also tried several natural fibers as substitutes for various components of automotive friction materials to improve their environmental impact [19, 20]. In order to better understand the contact evolution and the wear mechanisms occurring in a contact interface, it is also important to investigate both the sample and the counterpart surfaces after the execution of the experimental tests. Boz and Kurt [22] used a scanning electron microscope (SEM) to study the effect of Al_2O_3 on the friction performance of an automotive brake friction material. In general, much effort was made in the investigation of the morphology of the surfaces, analyzing phenomena such as the formation and destruction of the primary and secondary plateau [23–26]. Each mentioned study showed the effect of one or more ingredients on the behavior of a given friction material formulation. However, while these researches provide valuable qualitative insights regarding the tribological properties of the investigated ingredients, the quantitative accuracy of their results is limited to compositions and quantities similar to those employed in each respective study. This means that employing the same proportion of an ingredient investigated in the aforementioned studies will produce dissimilar quantitative results, depending on the specific composition of the remaining elements within the formulation of the friction material. Of course, this is well known, so designing a brake pad composition is challenging.

Besides the friction material ingredients, the braking parameters, such as sliding velocity, P_C, and temperature, also play an important role in determining the behaviour of a disc brake system, i.e., the COF and the wear. Many studies have been conducted to model brake friction couplings' behavior. These predictive analyses include investigations on the stresses and deformations that act on the system components [27, 28], the braking temperature [29, 30], the wear [28, 31, 32], and the COF [21, 33–35] achieved by the friction materials, and were carried out adopting different approaches, including finite element methods (FEM) and semi-empirical modelling. Although some interesting and relevant results were achieved, the predominant portion of these models is limited to the simulation stage and has not been subjected to experimental validation [33]. The models that were directly compared to experimental tests were built upon established and well-characterized compositions of friction materials. Consequently, these models do not offer significant advantages for designing a brake pad formulation from scratch. Instead, they primarily focus on examining the effects of some specific alterations on a predefined formulation.

To move towards a model capable of predicting the tribological properties of friction material from its formulation, Varriale et al. [21] proposed a cellular automaton (CA)-based simulation approach to evaluate

the brake system performance of two friction materials having different percentages of the same metals in the mixture. The model was calibrated using literature tribological data from Kumar and Bijwe [14], and afterward, two formulations differing in the steel fiber (SF) content were simulated and experimentally tested. The COF evolution of a braking event was satisfactorily predicted by the simulation model, despite the base composition used for its calibration being substantially unknown. The CA approach was chosen because of its better capability to simulate the mesoscopic processes that govern the tribological contact in brake pad friction materials, which occur at a scale lower than 500 μm and are therefore not suitable to be represented via the FEM approach [36]. The CA approach was first employed as a calculation tool by von Neumann [37], and since then, it has been employed in various fields, ranging from biology to physics [33]. As previously mentioned, CA is well suited for the correct representation of a tribological contact, and it has already been explored in the field of friction materials [38–42].

A CA simulation essentially works by discretizing the space, and thus the interacting materials themselves, in a regular cell lattice, while establishing functional rules and relationships between the cells [33]. The rules themselves will then depend on the characteristics of the material represented by each cell. Therefore, a correct and detailed representation of the simulated materials is required to increase the model's accuracy. In the case of brake pad friction materials, this is made difficult by the composite nature of the material itself, which contains many different ingredients that simultaneously interact at the contact surface. Hence, knowing the tribological behavior of each ingredient would be required to correctly establish the functional rules that govern the cell elements in the CA model.

Therefore, the final aim of the present research is to build a database of material tribological behaviors by conducting tribological characterization of the single ingredients employed in brake pad formulations via experimental testing. Correctly assessing the tribological behavior of different ingredients would allow for predicting the performance (i.e., COF and wear) of a friction material compound using an adaptation of the CA tool described in Ref. [21], without producing any pad prototypes. Consequently, this would considerably reduce development-related time and costs while also providing the capability to fine-tune a formulation for a specific application.

In light of these considerations, the study presented aims to investigate the tribological properties and the contact surface features of four ingredients belonging to different ingredient families of a copper-free friction material compound, performing PoD experimental tests and SEM analysis. This initial set of analyses aims to assess the feasibility of the approach through the simplified PoD results, providing a preliminary testbed for the CA model. The proposed approach involves the production of pin samples entirely made of the material of interest plus a binder agent, with the investigated material composing a predominant part of the mixture, to a degree which, to the best of the authors' knowledge, is unprecedented in the friction material field. A patent application for the sample production approach employed in this study has already been submitted. The production of such samples allows for a tribological characterization of the single ingredients more representative of the conditions they face in a braking system application, which, to the best of the authors' knowledge, has never been investigated at such detail before. Both samples and disc counterpart surfaces were analysed by SEM and energy-dispersive X-ray spectroscopy (EDXS) analyses. The evolution of the COF during the tests, its mean value, and the specific wear coefficient (K_a) for each ingredient and the counterpart discs were also evaluated.

2 Materials and methods

2.1 Materials

The materials employed in this study were aramid fiber (AF), SF, synthetic Gr, and silicon carbide (α-SiC), shown in Figs. 1 and 2, and novolac phenolic resin (Ph). Furthermore, a commercial copper-free low-metallic friction material powder mixture was also used. Each one of the provided ingredients was chosen to investigate the tribological behavior of one of the classes of ingredients of friction materials:

- AF and SF are reinforcing materials. Although they both enhance the mechanical and structural properties of the friction material composite, two

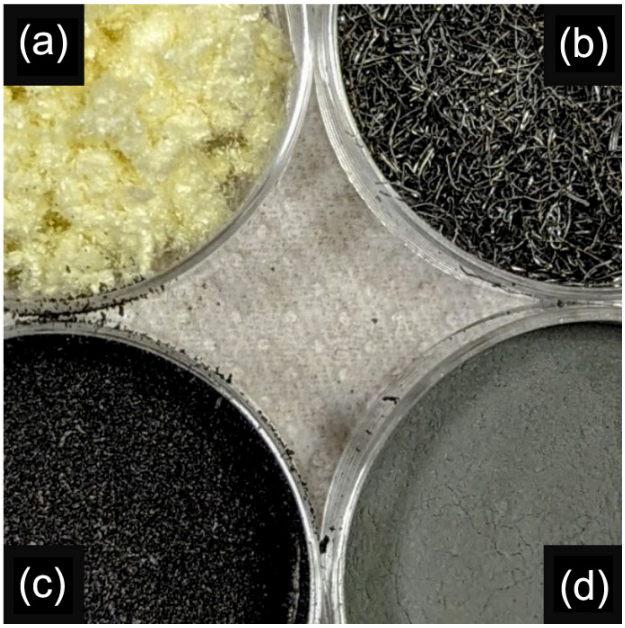

Fig. 1 Four main ingredients were investigated during this study: (a) AF, (b) SF, (c) Gr, and (d) SiC.

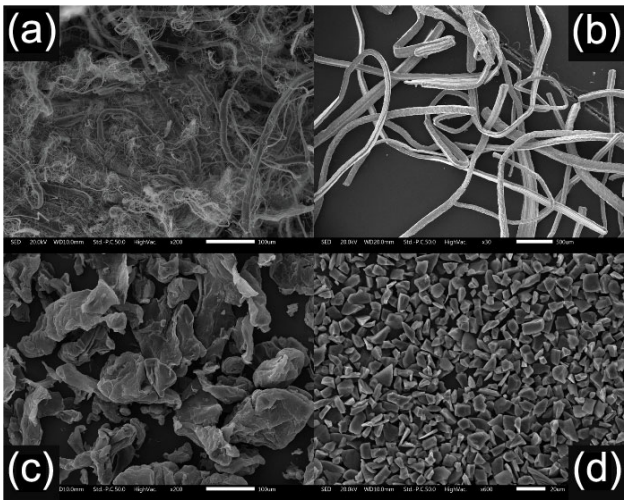

Fig. 2 Secondary electron detector SEM micrographs of (a) AF at 200× magnification, (b) SF at 30× magnification, (c) Gr at 200× magnification, and (d) SiC at 600× magnification.

different representatives of the reinforcing material class were chosen since they are expected to have different tribological behavior, due to their distinct nature. AF is an organic material, while SF is a metal.

- Gr is a solid lubricant.
- SiC is an abrasive.
- Ph is a binder. It serves the purpose of holding the other components together, effectively creating a polymer-matrix composite material.

Grey cast iron discs, extracted from real car disc brakes, were used as counterface. Note that this material was chosen because it is the most commonly used disc material in the automotive field. All ingredients and materials were supplied by Bergamo Co. Ltd.

2.2 Sample preparation

A total of six different compositions were produced. The volume fraction of the constituents and the codenames assigned to the produced sample compositions are listed in Table 1, while examples of specimens used for PoD tests (pins) are shown in Fig. 3.

The compositions 90AF, 90SF, 90Gr, and 80SiC were produced to investigate the tribological behavior of AF, SF, Gr, and α-SiC, respectively. Backscattered electrons detector SEM micrographs of the external surfaces of these samples are shown in Fig. 4. The samples appear well-compacted, with only 90SF (Fig. 4(b)) showing the presence of bigger pores. AF defibrillation can be appreciated in 90AF (Fig. 4(a)), while 90Gr (Fig. 4(c)) appears extremely compacted with negligible presence of microscopic pores. The original SiC particles are still discernible in 80SiC

Table 1 Volumetric fractions of ingredients employed for each of the produced compositions.

Codename	Ph (vol%)	AF (vol%)	SF (vol%)	Gr (vol%)	α-SiC (vol%)	Commercial mixture (vol%)
90AF	10	90	—	—	—	—
90SF	10	—	90	—	—	—
90Gr	10	—	—	90	—	—
80SiC	20	—	—	—	80	—
MIX	10	22.5	22.5	22.5	22.5	—
REF	—	—	—	—	—	100

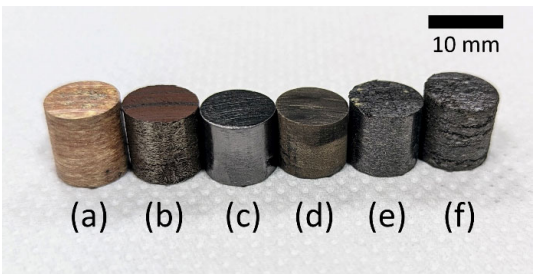

Fig. 3 Tested pin samples of each produced composition: (a) 90AF, (b) 90SF, (c) 90Gr, (d) 80SiC, (e) MIX, and (f) REF.

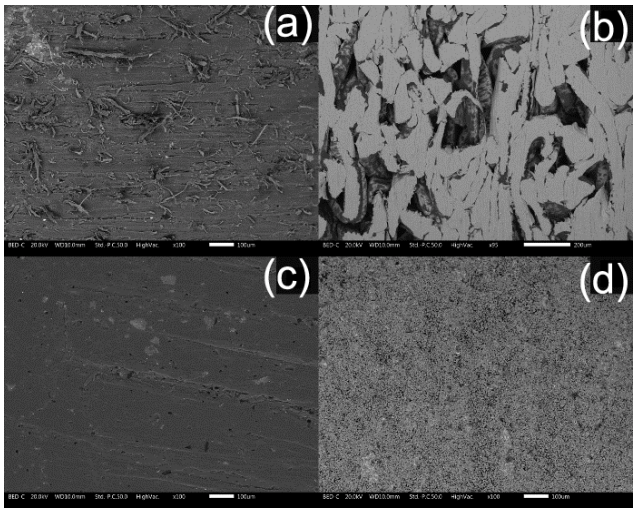

Fig. 4 Backscattered electrons detector SEM micrographs at 100× magnification of external surfaces of cylindrical pin samples of (a) 90AF, (b) 90SF, (c) 90Gr, and (d) 80SiC.

(Fig. 4(d)). Note that 80SiC is the only one among these four compositions having an 80% volume fraction of ingredients. This was dictated by preliminary tests not included in this manuscript, which showed insufficient structural resistance of samples with higher SiC content.

Although containing a fraction of Ph binder, these samples were considered representative of the behavior of their predominant ingredient to be used as calibration for a CA model. This consideration was based on two points:

- The predominant ingredient accounts for at least 90% of the contact area. This value is reduced to around 80% when abrasive ingredients such as SiC are used. This reduction is deemed acceptable due to the extreme difference in stiffness and the abrasive nature of SiC, which causes the abrasive ingredient to overshadow the soft Ph during interaction with a cast iron disc.
- A fraction of Ph similar, if not higher, to that employed for these samples, is always present in brake pad friction materials.

The MIX composition was produced to compare the individual contributions of the chosen ingredients with friction material comprising their mixture in equal parts, and it was not designed to be representative of conventional brake friction material.

Finally, the REF composition is a reference baseline for brake pad friction material. Note that the commercial friction material mixture comprises multiple ingredients, some listed in Table 2.

The compositions were designed considering the volumetric percentage of the components to control the fraction of contact area constituted by the main ingredient (AF, SF, Gr, and SiC), to investigate better and compare their contribution to the tribological properties of the sliding contact. To obtain the desired volumetric fractions, the required mass fractions were calculated considering the component densities listed in Table 3:

The sample production procedure for each composition was structured as follows:

- Mixing the composition for 15 min using a tubular (WAB T2F, WAB) to ensure a homogeneous distribution of each ingredient with the Ph binder.
- Hot pressing of the mixture in special tool steel molds using a mounting press (Pneumet I, Buehler), applying a molding pressure of 60 MPa for 15 min at 150 °C. This step allowed for obtaining cylindrical pin samples with a diameter of 10 mm.
- Curing the pins in a muffle furnace at 180 °C for 3 h to achieve complete binder crosslinking and bestow structural soundness to the samples.

Three specimens for each composition were produced following this procedure. The density and the porosity of each sample were evaluated following a procedure similar to that illustrated in ASTM B963-22. The only notable difference was that the weight

Table 2 Ingredients constituting commercial friction material composition.

Function	Constituent
Binder	Ph
Reinforcing fibers	Steel
Fillers	Vermiculite, others
Abrasives	α-SiC, magnesium oxide, and aluminum oxide
Lubricants	Gr, tin sulfide, and zinc oxide

Table 3 Densities of investigated ingredients. These values were used to calculate the quantities to be used in each formulation.

Density	Value (g/cm^3)
ρ_{Ph}	1.3
ρ_{AF}	1.4
ρ_{SF}	7.8
ρ_{Gr}	2.2
ρ_{SiC}	3.2

of the samples was taken in air and in water also before oil impregnation. The oil impregnation was performed after drying the samples in a ventilated oven at 110 °C for 2 h.

Cast iron disc surfaces were polished with SiC 180 grit abrasive paper and cleaned thoroughly with a special degreaser and acetone to remove any residual impurity, dirt, grease, or oil.

2.3 Experimental

2.3.1 Tribological characterization

The tribological characterization of the pins was performed by dry sliding tests against grey cast iron disc counterfaces using a PoD tribometer (DHM-600, Ducom). The testing rig is schematized in Fig. 5. The tests were performed at a sliding velocity (v_s) of 1.51 m/s under a nominal P_C of 1 MPa, which was achieved by applying a 79 N load (F_n) on the specimen. Each test lasted for a total duration of 90 min, except for 80SiC, in which case the test duration was lowered to 60 min due to the excessive wear of the samples recorded during preliminary tests, which could have damaged the testing equipment. Three specimens for each composition were tested following this procedure.

The PoD setup was chosen as preliminary exploration for this approach due to two main reasons:

- Lower time is required for the production and structural assessment of the cylindrical samples with respect to those required for the dynamometric bench setup. This allowed for the successful prototyping of the newly conceived samples
- Faster testing times, which were deemed valuable due to the preliminary nature of the work

Although the PoD conditions are not representative of the whole braking conditions spectrum, previous works in our laboratory showed a good correlation between the tribological behavior of friction materials tested on the PoD equipment and a reduced-scale dynamometric bench [43]. Moreover, a simpler PoD setup allows for an easier pre-validation of the CA modeling approach, which, if successful, can eventually be scaled up to the dynamometric bench level.

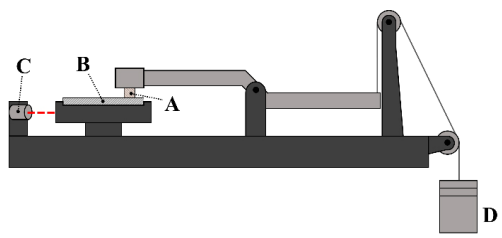

Fig. 5 Schematic representation of pin-on-disc equipment. Contact load is applied through a weight (D), which pushes the pin sample (A) against the rotating counterface disc (B). A pyrometer (C) measures the temperature of the disc holder.

Before testing, each sample underwent a run-in procedure to obtain a conformal contact between the pin and disc surfaces. This procedure consisted of a test run on the PoD tribometer under the same testing parameters used for the actual tests until the pin and the disc surfaces reached complete mutual contact (conformal contact).

During the test, the COF (μ) was calculated in real-time by measuring the friction force (F_t) through an IPA BR021H2 load cell, following Eq. (1):

$$\mu = \frac{F_t}{F_n} \tag{1}$$

where F_n is the applied normal force, which was set at 79 N by applying a weight (see Fig. 5, letter D). The load cell is embedded in the PoD equipment, and it is positioned such as to make contact with the PoD arm at the same distance of the tested pin concerning the pivotal point of the PoD arm, but on the opposite side, i.e., in order to experience a force identical to the tangential F_t acting on the pin.

The pin and disc mass was measured before and after every test using an analytical balance with a sensitivity of 10^{-1} mg. The wear of the samples was measured by calculating K_a, according to Archard's Wear law [44, 45]:

$$K_a = \frac{V_w}{F_n \cdot s} \tag{2}$$

where V_w is the volume of worn material; s is the total sliding distance. Three specimens were tested for each composition.

The temperature of the disc was monitored using the infrared (IR) thermal sensor built into the PoD rig (see Fig. 5, letter C). It is important to note that the sensor measures the temperature of the disc holder and not of the disc itself, and thus, the temperature measured by the equipment is not representative of

the actual value reached during contact, but it is still a valuable comparative measurement.

2.3.2 Worn surface characterization

The surfaces of the tested pins and discs were analyzed by a SEM (IT-300, JEOL). The SEM is also equipped with a dedicated sensor, which allows the use of EDXS on the surfaces of the samples to acquire quantitative elemental composition analyses and composition maps.

3 Results and discussion

3.1 Sample production

The average bulk density and porosity of each composition is shown in Table 4, along with the density calculated through a weighted average of its components (Table 3). All the prepared compositions showed a lower density than the calculated ones. This could be explained by the curing process of the Ph, which evolves some gaseous byproducts during its crosslinking, thus leading to an expansion of the material, mass loss, and the formation of voids in the final product [46–49]. This expansion could also be influenced by the morphology of the different ingredients, which might affect the structural response of the composite to the generated internal stresses. In fact, the volume of the produced pins increased from 2% to 15% after the curing step, depending on the composition. Of course, the different compaction capability of each ingredient might also play a role, due to their different morphology, physical, and mechanical properties. While the exact cause for the lower measured density was not specifically investigated, the volumetric porosity listed in Table 4 shows a good correlation with the difference between calculated and measured density, i.e., higher porosity values led to higher relative differences in the density.

Table 4 Calculated density of samples (through a weighted average of the density of its components), measured density, and volumetric porosity of produced samples.

Codename	Calculated density (g/cm^3)	Measured density (g/cm^3)	Porosity (vol%)
90AF	1.42	1.29±0.01	6.8±0.1
90SF	7.15	4.94±0.18	30.3±0.3
90Gr	2.11	1.88±0.02	0.5±0.1
80SiC	2.69	1.92±0.05	29.8±0.4
MIX	3.40	2.79±0.03	3.5±0.2
REF	—	2.17±0.06	21.2±0.5

3.2 Tribological testing

The average COF curves of each composition, recorded during PoD testing, are shown in Fig. 6. The friction coefficient of 90AF, 90Gr, 80SiC, MIX, and REF rapidly increased at the very beginning of the test, eventually reaching a plateau. This behavior is common in sliding interaction between materials [23, 50–55], and is composed of an initial run-in stage that then leads to a steady-state regime. The run-in stage takes place due to different possible phenomena, such as an increase in the real contact area or the formation of a layer of transferred material on the mating surfaces [23, 50].

90SF displayed the same initial run-in phase, however, its COF started to decline right after reaching an early maximum peak, although its curve started to flatten out towards the end of the test. Differently from the other investigated samples, the high steel content of 90SF has great chemical compatibility with the cast iron counterface, which leads to a high work of adhesion value. The work of adhesion W_{12} between two materials can be evaluated using experimental equations such as Eq. (3) [50, 56], and it is proportional to the adhesion force exerted by two surfaces in contact, which is in turn, proportional to the friction coefficient.

$$W_{12} = c \cdot (\gamma_1 + \gamma_2) \tag{3}$$

where W_{12} is the work of adhesion between materials 1 and 2; γ_1 and γ_2 are the surface energies of materials 1 and 2, respectively; c is an experimental constant proportional to the chemical compatibility of the materials in contact. Values of c for different material couplings can be found on experimental charts, such as those provided by Rabinowicz [56]. Therefore, 90SF showed the highest recorded μ value at the beginning of the test. However, the oxidation of the interacting metals under adhesive wear, the formation

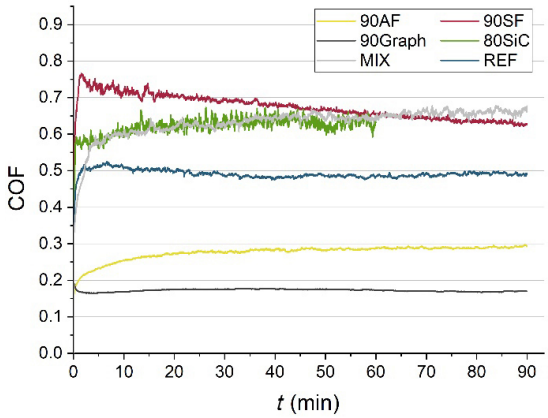

Fig. 6 Average COF curves obtained by PoD testing.

of an oxidized friction layer, and the interplay of different friction mechanisms, such as tribo-oxidation, lowered its friction coefficient over time. This is a known phenomenon in the tribology field, which mainly occurs in the case of metal–metal contacts, and the lowering of the COF is usually also accompanied by a lowering of the wear rate [57, 58].

Some of the average PoD tribological results and their standard deviations are reported in Table 5. Since the steady-state regime is not a fixed and pre-defined timeframe, the starting point of the steady-state regime was set manually for each tested specimen.

Along with their lower μ value, 90AF and 90Gr showed the lowest pin wear, represented by the specific wear coefficient of the pin ($K_{a,pin}$) in Table 5. The low adhesion between the pin material and the cast iron disc, paired with the softness of the sample ingredients, allowed for sliding contact with a very low presence of adhesive and abrasive wear. For the same reasons, 90AF and 90Gr also showed the lowest wear of the disc, represented by the specific wear coefficient of the disc ($K_{a,disc}$) reported in Table 5. In particular, their disc wear appeared to be practically negligible, which was expected since the cast iron disc counterface is substantially harder than the constituents of the aforementioned pins, i.e., AF, Gr, and Ph. The lowest values of μ, $K_{a,pin}$, and $K_{a,disc}$ were all registered in the case of 90Gr, which was expected due to its solid lubricant nature.

Table 5 Average tribological results obtained through PoD testing.

Codename	$\mu_{steady\text{-}state}$	$K_{a,pin}$ (10^{-14} m^2/N)	$K_{a,disc}$ (10^{-14} m^2/N)	$T_{MAX,disc}$ (°C)
90AF	0.29±0.02	0.39±0.05	0.00±0.00	42±1
90SF	0.65±0.03	1.31±0.29	1.09±0.11	56±4
90Gr	0.17±0.01	0.14±0.02	0.00±0.00	39±1
80SiC	0.63±0.03	36.03±6.32	8.32±0.42	56±4
MIX	0.65±0.02	2.64±0.34	2.36±0.12	53±2
REF	0.49±0.01	2.81±0.14	1.46±0.11	47±2

The 90SF pin wear was higher than 90AF and 90Gr, but interestingly lower than MIX and REF. As previously discussed, the sustained tribological pairing of almost pure steel with the cast iron counterface is likely to have induced the formation of an oxidized third-body layer and the oxidation of the mating material surfaces themselves. These oxidized films could then act as a protective shield for the two parent materials. This is a known phenomenon, essentially caused by the transition from adhesive wear to tribo-oxidative wear during the sliding interaction [50]. However, it is also important to note that the oxide layers can only bestow wear-resistance properties while working under non-critical conditions. In fact, under harsher operating conditions, the oxide might fail, exposing the parent material to the same reiterative oxidation and destruction process, which would then be detrimental to the wear properties [50, 58]. For the same reason, the wear of the disc was lower in the case of 90SF with respect to MIX and REF. In fact, the presence of different ingredients could hinder the formation of a fully-oxidized interface. In particular, the abrasive ingredients in the MIX and REF compositions are prone to wear the cast iron disc surface and any oxide layer that could form on the interacting surfaces.

MIX and REF displayed comparable pin wear, but the disc wear was substantially lower for REF, which was expected since its composition is an optimized commercial mixture. Notably, since the COF was higher in the case of MIX, it was apparent that the amount of lubricant was not enough to compensate the contribution of the abrasive SiC powder.

Unsurprisingly, 80SiC showed the highest disc wear. The SiC powder is much harder than the cast iron disc, which is easily worn by this abrasive interaction. As anticipated in Section 2.3.1, the wear of the 80SiC pins was even more severe, to such an extent that the test duration had to be restricted to 1 h to avoid damaging the PoD equipment. This result can be

explained by the low adhesion with the polymeric matrix [59] and the dimension of the SiC particles that constitute the abrasive powder. Its granulometry is in fact very fine (below 30 μm), which means that at the sliding interface, under the harsh contact stresses, each interacting SiC particle does not have an anchoring body with sufficient dimensions to hold it to the pin polymeric matrix, and is therefore prone to be removed from the surface. Furthermore, the SiC particles have a very sharp morphology (Fig. 2(d)), which induces stress concentration effects and further weakens their bonding to the pin matrix [59].

Figure 7 shows, for each tested composition, the profilometer curve obtained by probing the wear track of the disc perpendicularly to the sliding direction. The curves corroborate the observations made regarding the disc wear of the different materials, showing that 80SiC produces the deepest wear track, followed by MIX, REF, and 90SF. Notably, 90AF and 90Gr are not proper wear tracks but appear as transfer layers of the pin material on top of the disc surface. As previously discussed, AF and Gr are softer than cast iron and are thus bound to be worn by the disc material. In these cases, the pin material accumulates onto the disc forming a transfer layer. This consideration is coherent with the results and observations made in this section, where it was noted that the $K_{a,disc}$ value of 90AF and 90Gr was practically negligible.

3.2.1 *Temperature and wear relationship*

The maximum temperature values reached by the disc $T_{MAX,disc}$ reported in Table 5 were measured by an IR sensor pointed at the disc holder of the PoD equipment (Fig. 5, letter C). Due to its positioning, the recorded $T_{MAX,disc}$ values are lower than the actual temperature of the disc. Indeed, other studies show how higher contact temperatures are reached when operating in similar sliding conditions [6]. Although the values themselves may not be quantitatively accurate, their comparison still illustrates the different behaviors of the tested compositions.

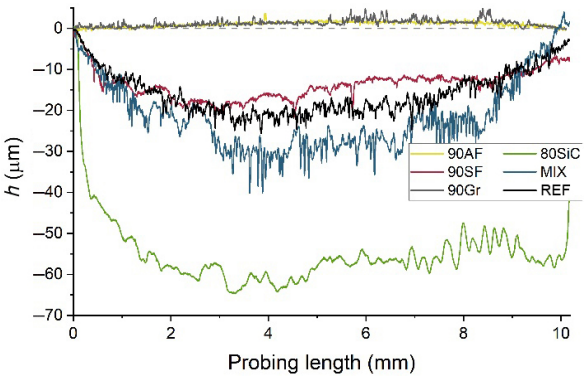

Fig. 7 Profilometer curves of worn surfaces of disc for each tested pin composition.

The maximum temperature reached by the disc is closely related to the COF of the materials. In fact, a higher value of $\mu_{steady\text{-}state}$ led to higher registered $T_{MAX,disc}$, with MIX being the only exception but just by a small margin. The explanation for this observed result is fairly straightforward: the power dissipated by friction, which is converted to heat, is directly proportional to the friction coefficient, following Eq. (4):

$$P_{diss} = \mu \cdot F_n \cdot v_s \tag{4}$$

where P_{diss} is the dissipated power and v_s is the sliding speed. This equation embodies the working principle of a disc brake system, designed to dissipate the kinetic energy by converting it into heat. As explained in Section 2.3.1, F_n and v_s are fixed test parameters; therefore, the friction coefficient is the only variable in Eq. (4) that changes among the tested materials.

Although higher $\mu_{steady\text{-}state}$ values indeed led to higher disc temperatures, they did so in a non-proportional way. For example, 90Gr showed a friction coefficient close to a quarter of that of 90SF, but the 90Gr $\Delta T_{MAX,disc}$ respect to the laboratory ambient temperature of 25 °C was about half of that of 90SF. A number of different phenomena could be playing a role in this result, such as the different thermal properties of the pin materials (specific heat and thermal conductivity) that influence how the heat is distributed between the pin and the disc, and how efficiently it is dissipated from the contact region. However, during this study, there was also a correlation with the wear of the whole system, i.e., the wear of both the pin and the disc.

Figure 8 shows the correlation between the $\Delta T_{MAX,disc}/\mu_{steady\text{-}state}$ ratio and the specific wear coefficient of the system ($K_{a,system}$). The ratio between $\Delta T_{MAX,disc}$ and $\mu_{steady\text{-}state}$ represents how many degrees Celsius of temperature increase are produced by every unit of COF of the material, while the sum of $K_{a,pin}$ and $K_{a,disc}$ simply gives $K_{a,system}$. Note that 80SiC is not represented

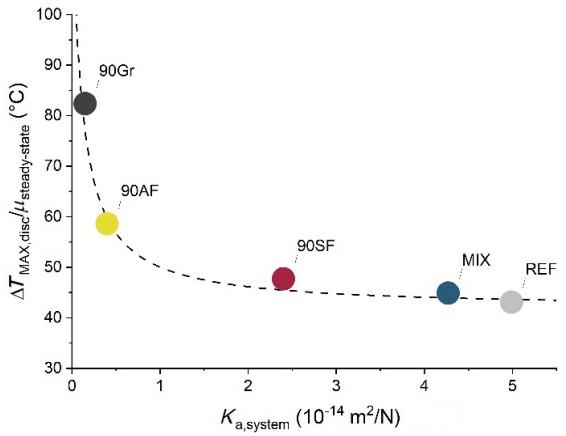

Fig. 8 Relationship between system wear and temperature generated per unit of friction coefficient of the material. Dashed line represents a hyperbolic interpolation of the results.

in Fig. 8 due to its too high K_a value (Table 5), which would lead to disproportionate axis scaling of the graph, specifically making 90SF, MIX, and REF appear as overlapping points. A hyperbolic curve, shown in Fig. 8, was found to fit best the correlation between $\Delta T_{MAX,disc}/\mu_{steady\text{-}state}$ ratio and $K_{a,system}$, suggesting that the proportionality between the COF and the heat production explained in Eq. (4) changes when introducing a considerable amount of wear. This does not mean that Eq. (4) is incorrect, but that the P_{diss} is converted into heat and consumed by the wear-related processes. In fact, the production of wear debris involves dissipation of some energy into superficial energy; thus, a higher wear amount would suggest a larger amount of energy dissipated through this mechanism. Moreover, other dissipation mechanisms could be taking place, such as the work necessary for the plastic deformation of the interacting material surfaces and the produced wear debris.

Of course, different materials will distribute the dissipated energy differently between heat, material deformation, and surface energy creation by debris production, and this partitioning might also depend on the contact conditions (i.e., stress and temperature). Furthermore, as previously mentioned, the thermal properties also play a role in the temperature increase of the disc.

Anyhow, the correlation shown in Fig. 8 only indicates the hypothesized phenomena. In fact, K_a is only representative of the V_w, and not of the dimension of the produced wear fragments, and therefore does not yield any information about the newly produced surfaces and thus about dissipated surface energy, produced by the wear process.

Although interesting, this topic was not further investigated in the present work because it is beyond the scope of the study.

3.2.2 *MIX behavior*

The MIX composition was purposely designed with identical volumetric fractions of its four main ingredients, i.e., AF, SF, Gr, and α-SiC, to compare its tribological behavior to those of the single ingredients. In particular, the MIX composition was designed to show how the tribological behavior of a friction material composite results from synergistic interactions between its ingredients, and it is not given by a simple averaging of the properties of its ingredients. Consequently, the MIX composition was not conceived as a realistic brake friction material composition.

The tribological properties that would have been obtained if each ingredient independently and equally contributed to the tribological properties of the mixture were therefore calculated and compared to those obtained through PoD testing. By averaging the contribution of each ingredient to any tribological property ($p_{MIX,predicted}$) of MIX, the value of that property could be calculated by Eq. (5):

$$p_{MIX,predicted} = \frac{p_{AF} + p_{SF} + p_{Gr} + P_{SiC}}{4} \quad (5)$$

where p_{AF}, p_{SF}, p_{Gr}, and p_{SiC} refer to one of the tribological properties of 90AF, 90SF, 90Gr, and 80SiC, respectively. Following Eq. (5), the predicted values of some tribological properties of the MIX composition were calculated, shown in Table 6 together with the actual measured properties.

The predicted properties substantially differ from those measured by PoD testing, except for disc wear. The friction coefficient $\mu_{steady\text{-}state}$, indicative of the braking power of a friction material, results in 48% higher than predicted while also obtaining a $K_{a,pin}$ 72% lower than anticipated. Although the actual maximum disc temperature $T_{MAX,disc}$ exceeds that calculated following Eq. (5) due to the lower expected COF, the measured $\Delta T_{MAX,disc}/\mu_{steady\text{-}state}$ ratio is lower than the predicted one. Note that a material producing

Table 6 Measured and predicted (considering the equal contribution of each ingredient) tribological properties of the MIX composition.

	$\mu_{\text{steady-state}}$	$K_{\text{a,pin}}$ (10^{-14} m^2/N)	$K_{\text{a,disc}}$ (10^{-14} m^2/N)	$T_{\text{MAX,disc}}$ (°C)	$\Delta T_{\text{MAX,disc}}/\mu_{\text{steady-state}}$ (°C)
MIX_{PoD}	0.65	2.64	2.36	53	43.1
$\text{MIX}_{\text{predicted}}$	0.44	9.47	2.35	48	52.3

the same COF as MIX, but having the $\Delta T_{\text{MAX,disc}}/\mu_{\text{steady-state}}$ ratio of $\text{MIX}_{\text{predicted}}$, would show a maximum disc temperature of about 59 °C. Therefore, it is evident how the interplay of the ingredients does not lead to a simple superposition of their properties but to a synergistic interaction.

Interestingly, the predicted disc wear $K_{\text{a,disc}}$ showed close agreement with the measured one. While this result might suggest that the previously mentioned synergistic effect of the ingredients in the composition only holds for the friction material pin, it is important to note that the measured disc wear matched the predicted one while producing almost 50% higher braking power.

As expected, Eq. (5) was not adequate to predict the behavior of the friction material comprising multiple different ingredients, highlighting the need for a more refined model.

3.3 Surface characterization

Figure 9 shows the surface of the discs after PoD testing against single-ingredient pins. The wear tracks are clearly visible, and distinct features characterize the different pin counterfaces.

As noted in Section 3.2, 90AF (Fig. 9(a)) and 90Gr (Fig. 9(c)) did not produce proper wear tracks but transferred layers on top of the cast iron disc. However, the presence of these transfer layers suggests that the μ values obtained through PoD testing (see Fig. 6 and Table 5) do not strictly arise from the sliding interaction between the pin and disc materials, but are also influenced by adhesive interactions between the pin surface and the pin material transferred on the disc surface. Therefore, the COF of 90AF was presumably increased by the formation of an aramid transfer layer, due to an enhancement of the chemical compatibility of the mating surfaces, which would cause an increase of the c parameter (see Eq. (3)) and thus of the work of adhesion. In the case of 90Gr, the formation of a transfer layer did not strongly affect

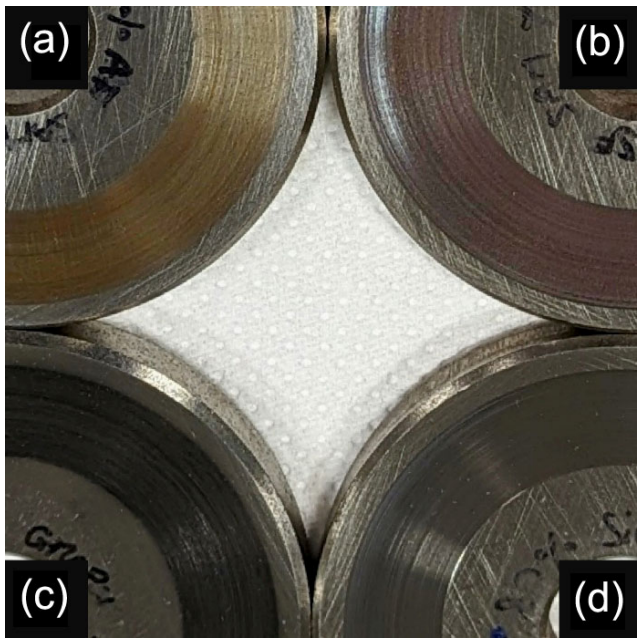

Fig. 9 Wear tracks and transfer layers on cast iron discs caused by the interaction, during PoD testing, with the four main ingredients investigated during this study: (a) AF, (b) SF, (c) Gr, and (d) SiC.

the COF, possibly leading to a slightly lower value. The solid lubricant role of Gr is in fact attributed to its layered structure, characterized by low adhesion between each layer [50, 60], thus easing the relative sliding motion. Therefore, the formation of a Gr transfer layer onto the disc surface should not cause an increase in the adhesive interaction between the pin and the disc.

Furthermore, the transfer layer could have influenced the COF by altering the deformation component towards energy dissipation since the elastic properties of the surfaces in contact were changed, as shown in Eq. (6) [61]:

$$\lim_{t\to\infty}(\mu(t)) = (\beta \cdot P_{\text{C}} + \tau)/P_{\text{C}} \tag{6}$$

where P_{C} is the contact pressure, and β and τ are two parameters related to the deformation and the adhesion components of friction. Therefore, τ is

somewhat proportional to W_{12} expressed in Eq. (3), and consequently to the chemical compatibility between the contacting materials. However, the adhesion component τ becomes more impactful than β for determining the COF value reached during sliding [61], especially since wear for 90AF and 90Gr was extremely low.

The wear track of 90SF (Fig. 9(b)) displays a reddish coloring, characteristic of hematite. The same color could be observed on the surface of the 90SF pins (Fig. 3), indicating oxidation of both mating surfaces, which would agree with the results and observations discussed in Section 3.2. SEM analysis further corroborated this hypothesis, showing strong oxidation of the iron present in both the pin and disc surfaces. Figure 10 shows SEM micrographs of the 90SF pin and disc surfaces obtained by the BSE detector and the respective EDXS maps of oxygen and iron. The surfaces of the pin (Fig. 10(a)) and of the disc (Fig. 10(d)) appear similar, showing the widespread presence of darker grey tones that indicate the presence of oxidation. This is confirmed by the EDXS maps of O (Figs. 10(b) and 10(e)), which is found all over the two surfaces. Furthermore, the darker patches, which are most discernible on the pin surface (see outlined shape in Figs. 10(a)–10(c)), show the presence of structures akin to those of the friction layers found on brake friction materials [23, 52]. These friction layers, or secondary contact plateaus, essentially form by accumulating and complying wear particles, which are oxidized during the sliding interaction through tribo-oxidation, producing a third body layer interposed between the original mating surfaces. Indeed, the darker regions on the BSE micrographs correspond to, respectively, brighter and darker regions on the O (Fig. 10(b)) and Fe (Fig 10(c)). EDXS maps, thus implying stronger oxidation of iron in those areas. The good tribological performance obtained by 90SF, i.e., low wear along with high COF (Table 5), suggests that the capability to form a stable, protective friction layer is indeed of paramount importance for the properties of a friction material. Notably, for a conventional brake pad friction material, the typical composition of its friction layer comprises different iron oxides, with a stronger presence of magnetite over hematite [62–64].

80SiC produced a "clean" wear track, as shown in Fig. 9(d), meaning that no oxidation nor exchange of material between the mating surfaces could be macroscopically observed, neither by the naked eye nor through optical microscopy. SEM analysis of the disc surface confirmed this hypothesis, only showing a scarce but widespread presence of Si on the wear track. Figure 11 shows the BSE micrograph and the corresponding EDXS maps of Si and Fe of the 80SiC pin surface. The presence of transferred patches of Fe

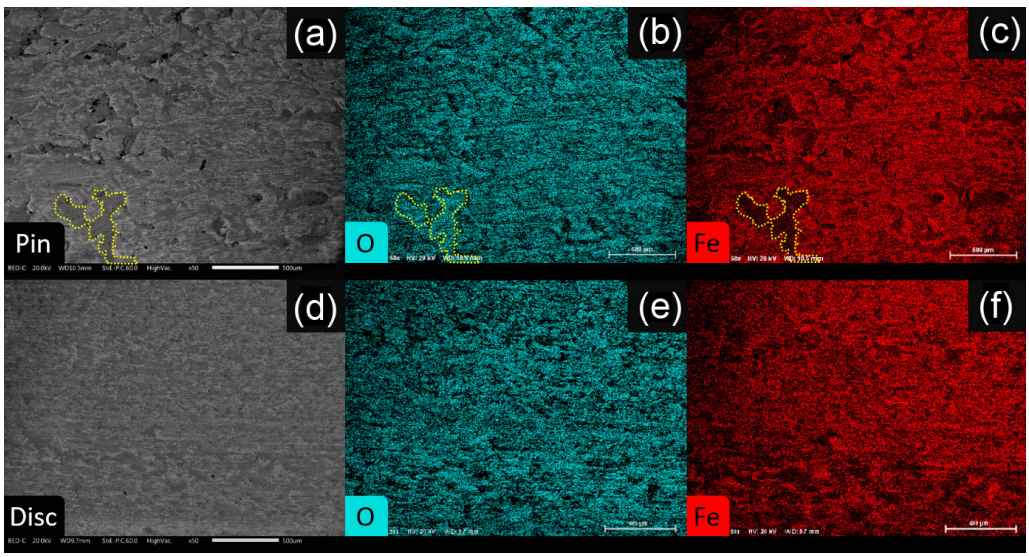

Fig. 10 Backscattered electrons detector SEM micrographs at 50× magnification of (a) a 90SF pin and (d) disc tested sample surface. EDXS maps of (b, e) oxygen and (c, f) iron acquired in the same areas are also shown. The yellow outline highlights one of the secondary contact plateaus formed on the pin surface.

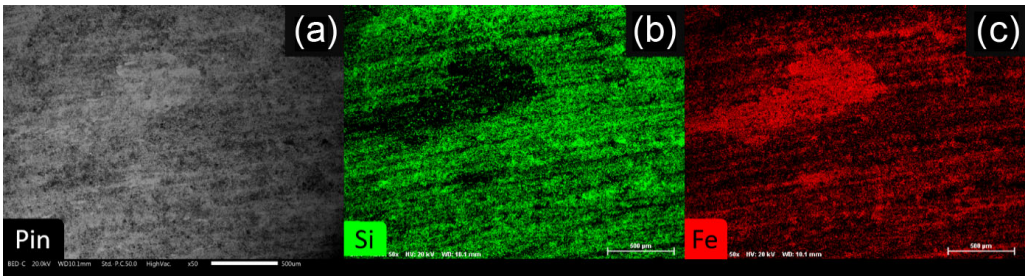

Fig. 11 (a) Backscattered electrons detector SEM micrograph at 50× magnification of an 80SiC pin sample tested surface. The EDXS maps of (b) silicon and (c) iron acquired in the same area are also shown.

from the cast iron disc is visible on the Fe EDXS map (Fig. 11(c)). This result is consistent with those of 90AF and 90Gr and also with the theory of adhesion, according to which the softer material is the one that is most likely transferred on the surface of the harder one. In the case of 80SiC, the presence of iron on the pin surface probably did not contribute much to the tribological behavior of the system (namely μ and K_a), primarily due to the significantly high wear of the pin.

Figure 12 shows the backscattered electrons detector SEM micrographs of the cross-section of the contact surface of the main-ingredient pins. 90AF (Fig. 12(a)) and 90Gr (Fig. 12(c)) do not show any noteworthy feature, which was expected since those materials were worn and transferred onto the mating surface. The micrographs of 90SF (Fig. 12(b)) and 80SiC (Fig. 12(d)) instead support the previous SEM observations. 90SF shows the presence of thick secondary contact plateaus (see outlined shape in Fig. 12(b)) that are accumulated and compacted between the SFs. EDXS analysis confirmed that these secondary contact plateaus are composed of oxidized iron.

In the case of 80SiC, spotting some very thin layers on the top of the contact surface (bright particles highlighted in Fig. 12(d)) was possible. Figure 13 shows the EDXS mapping of Fe and the corresponding BSE micrograph, which was taken on the region highlighted in Fig. 12(d). As can be seen from Fig. 13(b), the thin layer on the top of the contact surfaces is composed of iron particles, i.e., the cross sectional view of a patch akin to that observed in Fig. 11(c). It is evident that these particles were not able to be compacted into thicker secondary contact plateaus, thus further supporting the observation made regarding Fig. 11, stating that the iron transfer

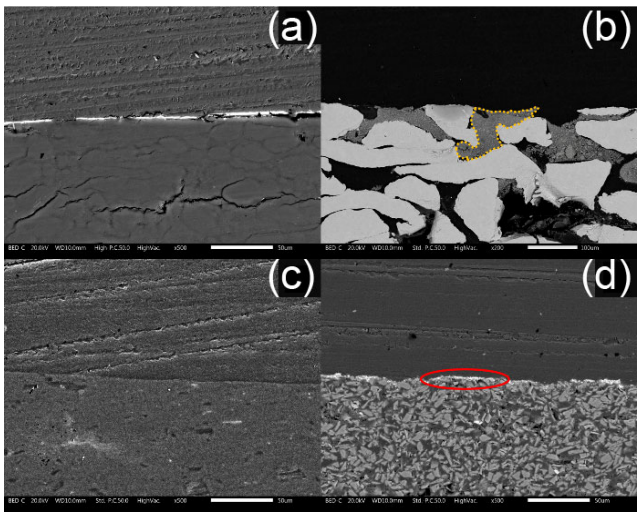

Fig. 12 Backscattered electrons detector SEM micrographs at 500× magnification of cross section of pin contact surface of (a) 90AF, (b) 90SF, (c) 90Gr, and (d) 80SiC.

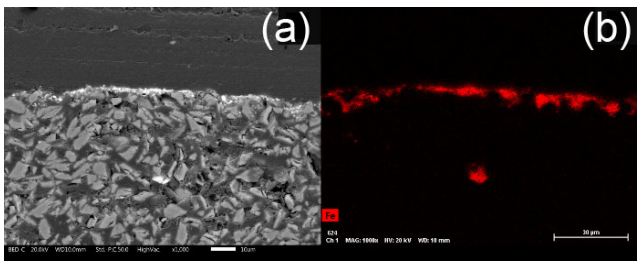

Fig. 13 (a) Backscattered electrons detector SEM micrograph at 1,000× magnification of 80SiC contact surface. The corresponding EDXS map of iron is also shown in (b).

onto the pin surface was unlikely to have had a meaningful contribution to the tribological properties of 80SiC.

Figure 14 shows the SEM BSE micrographs obtained for the MIX and REF compositions' pin and disc wear surfaces. The wear surface of the MIX composition showed similar features to those of REF, both in the pin and disc case.

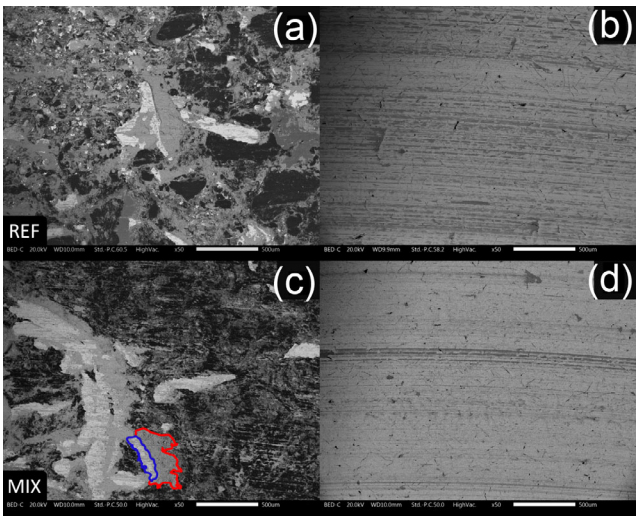

Fig. 14 Backscattered electrons detector SEM micrographs at 50× magnification of tested surface of (a) REF composition pin, (b) REF composition disc,(c) MIX composition pin, and (d) MIX composition disc. The blue and red outlines in (c) highlight an example of primary and secondary contact plateaus, respectively.

The pin surfaces of MIX and REF are characterized by the presence of a developed friction layer, comprising metallic primary contact plateaus (blue outline in Fig. 14(c)), which accommodate and support the accumulation and compaction of oxidized wear debris forming the secondary contact plateaus (red outline in Fig. 14(c)). Predictably, the surface of the REF pin shows more complexity due to multiple ingredients, while MIX's surface is binarily divided between the friction layer and the other ingredients. As confirmed by EDXS analysis of the surface, shown in Fig. 15, the darker region of the MIX pin (Fig. 14(c)) includes the carbonaceous ingredients (i.e., AF and Gr), SiC, and some small iron oxide patches. The SFs correspond to the lightest regions in the micrograph Fig. 14(c) and in the map Fig. 15(d) and act as primary contact plateaus, showing a behavior congruent with the previously discussed 90SF one.

The REF and MIX disc surfaces show the formation of secondary contact plateaus extending in the sliding direction. These plateaus appear as lines darker than the light-cast iron background in the BSE micrographs shown in Figs. 14(b) and 14(d). Secondary contact plateaus form along lines on the surface of the discs because the agglomeration and compaction of the oxidized debris are favored inside the grooves [58] that are formed in the sliding direction. In the case of the REF wear track, these contact plateaus cover a larger portion of the surface, denoting a better capability to sustain the formation of more stable contact plateaus concerning the MIX composition. This is congruent with the considerations made in Section 3.2 regarding the higher disc wear of MIX concerning that of REF (Table 5), which could be explained by the considerable amount of SiC in its composition. Indeed, the abrasive SiC powder can wear the surface of the disc and the oxide plateaus that form on top of it, leading to higher disc wear and lower plateau coverage on the wear track. Furthermore, this would also explain the higher COF obtained by MIX, enabled by stronger abrasive friction and increased metal–metal contact by removing oxide layers.

The tribological data collected in this investigation, along with information from the characterization analyses, will be crucial for developing the CA model. CA discretizes the material's surface in a finite number of cells, each with properties depending on the material they represent. Within any given time frame, the state of each cell is determined not only by its current material properties but also by the interactions with adjacent cells. Consequently, the surface cell lattice will initially be determined by the mixture composition and will evolve based on the interactions between cells. The effect of every interaction will be modeled around the data hereby obtained, i.e.,

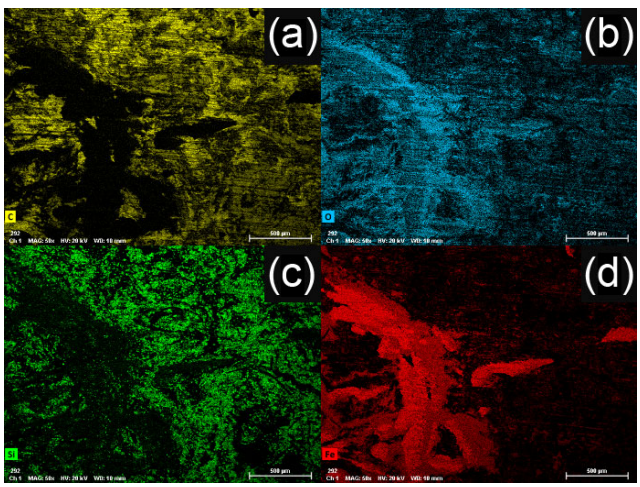

Fig. 15 EDXS maps at 50× magnification of the contact surface of the MIX composition, showing the distribution of (a) carbon, (b) oxygen, (c) silicon, and (d) iron. The corresponding BSE micrograph is shown in Fig. 14(c).

contribution to the COF, likeliness to wear out, direction of material transfer, etc.

The investigation of the MIX composition allows for a fundamental preliminary representation of surface conditions that need to be represented by the CA model in scenarios involving interactions among multiple ingredients. Consequently, its tribological results will be used as the first testbed for the model, thus serving as a valuable initial calibration tool.

4 Conclusions

This work is intended as a preliminary study for the development of a cellular automaton (CA) predictive model to improve the design process of brake pad friction materials. To accomplish this, the tribological characterization of materials representative of the main classes of brake pad friction material ingredients was performed through PoD testing, allowing for a more comprehensive understanding of their behavior during a sliding interaction with a cast iron disc. The materials investigated were aramid fiber (AF) and steel fiber (SF) as reinforcing materials, graphite (Gr) as solid lubricant, and silicon carbide (α-SiC) as abrasive.

Developing a production process for novel tribological test samples predominantly composed of a single ingredient was successful. The interaction between the pin materials and the cast iron disc led to an evolution of the contact conditions and features, which depended on the characteristics of the ingredients, often leading to the formation of a third body mainly produced by the material transfer between the two mating surfaces. This phenomenon altered the properties of the tribological pairings in different ways depending on the involved materials, sometimes leading to unexpected values of COF and wear. Furthermore, a relationship between the temperature increase and the wear of the different materials was observed. The tribological values obtained for the investigated materials and the observed interaction between the different mating surfaces constitute valuable data for developing the governing functional rules required for the conceived CA model.

Future activities related to this study will deal with the production and testing of other ingredients, their testing in different conditions, and the development of the predictive CA model using the obtained tribological data.

Acknowledgements

This research received no specific grant from funding agencies in the public, commercial, or not-for-profit sectors. Supplies were provided by Brembo SpA.

Declaration of competing interest

The authors have no competing interests to declare that are relevant to the content of this article.

References

[1] Liu H L, Cha Y Y, Olofsson U, Jonsson L T I, Jönsson P G. Effect of the sliding velocity on the size and amount of airborne wear particles generated from dry sliding wheel–rail contacts. *Tribol Lett* **63**(3): 30 (2016)

[2] Cha Y Y, Hedberg Y, Mei N X, Olofsson U. Airborne wear particles generated from conductor rail and collector shoe contact: Influence of sliding velocity and particle size. *Tribol Lett* **64**(3): 40 (2016)

[3] Wahlström J, Olander L, Olofsson U. A pin-on-disc study focusing on how different load levels affect the concentration and size distribution of airborne wear particles from the disc brake materials. *Tribol Lett* **46**(2): 195–204 (2012)

[4] Wahlström J, Söderberg A, Olander L, Jansson A, Olofsson U. A pin-on-disc simulation of airborne wear particles from disc brakes. *Wear* **268**(5–6): 763–769 (2010)

[5] Wahlström J, Gventsadze D, Olander L, Kutelia E, Gventsadze L, Tsurtsumia O, Olofsson U. A pin-on-disc investigation of novel nanoporous composite-based and conventional brake pad materials focussing on airborne wear particles. *Tribol Int* **44**(12): 1838–1843 (2011)

[6] Wahlström J, Lyu Y Z, Matjeka V, Söderberg A. A pin-on-disc tribometer study of disc brake contact pairs with respect to wear and airborne particle emissions. *Wear* **384–385**: 124–130 (2017)

[7] Gomes Nogueira A P, Carlevaris D, Menapace C, Straffelini G. Tribological and emission behavior of novel friction materials. *Atmosphere* **11**(10): 1050 (2020)

[8] Lyu Y Z, Leonardi M, Wahlström J, Gialanella S, Olofsson U. Friction, wear and airborne particle emission from Cu-free brake materials. *Tribol Int* **141**: 105959 (2020)

[9] European Commission. Proposal for a Regulation of the European Parliament and the Council on type-approval of motor vehicles and engines and of systems, components and separate technical units intended for such vehicles, with respect to their emissions and battery durability (Euro 7) and repealing Regulations (EC) No 715/2007 and (EC) No 595/2009. 2022. Available at https://eur-lex.europa.eu/legal-content/EN/TXT/?uri=CELEX:52022PC0586

[10] Chan D, Stachowiak G W. Review of automotive brake friction materials. *P I Mech Eng D-J Aut* **218**(9): 953–966 (2004)

[11] Xiao X M, Yin Y, Bao J S, Lu L J, Feng X J. Review on the friction and wear of brake materials. *Adv Mech Eng* **8**(5): 168781401664730 (2016)

[12] Zhao X G, Ouyang J, Yang H M, Tan Q. Effect of basalt fibers for reinforcing resin-based brake composites. *Minerals* **10**(6): 490 (2020)

[13] Bagheri Kazem Abadi S, Khavandi A, Kharazi Y. Effects of mixing the steel and carbon fibers on the friction and wear properties of a PMC friction material. *Appl Compos Mater* **17**(2): 151–158 (2010)

[14] Kumar M, Bijwe J. Composite friction materials based on metallic fillers: Sensitivity of μ to operating variables. *Tribol Int* **44**(2): 106–113 (2011)

[15] Kumar M, Bijwe J. Non-asbestos organic (NAO) friction composites: Role of copper; its shape and amount. *Wear* **270**(3–4): 269–280 (2011)

[16] Cho M H, Ju J, Kim S J, Jang H. Tribological properties of solid lubricants (graphite, Sb_2S_3, MoS_2) for automotive brake friction materials. *Wear* **260**(7–8): 855–860 (2006)

[17] Zheng D, Zhao X, An K, Chen L, Zhao Y, Khan D F, Qu X H, Yin H Q. Effects of Fe and graphite on friction and wear properties of brake friction materials for high-speed and heavy-duty vehicles. *Tribol Int* **178**: 108061 (2023)

[18] Mahale V, Bijwe J, Sinha S. Influence of nano-potassium titanate particles on the performance of NAO brake-pads. *Wear* **376–377**: 727–737 (2017)

[19] Milosevic M, Valášek P, Ruggiero A. Tribology of natural fibers composite materials: An overview. *Lubricants* **8**(4): 42 (2020)

[20] Gehlen G S, Nogueira A P G, Carlevaris D, Barros L Y, Poletto J C, Lasch G, Straffelini G, Ferreira N F, Neis P D. Tribological assessment of rice husk ash in eco-friendly brake friction materials. *Wear* **516–517**: 204613 (2023)

[21] Varriale F, Riva G, Wahlström J, Lyu Y Z. A mesoscopic simulation approach based on metal fibre characterization data to evaluate brake friction performance. *Lubricants* **10**(3): 34 (2022)

[22] Boz M, Kurt A. The effect of Al_2O_3 on the friction performance of automotive brake friction materials. *Tribol Int* **40**(7): 1161–1169 (2007)

[23] Eriksson M, Jacobson S. Tribological surfaces of organic brake pads. *Tribol Int* **33**(12): 817–827 (2000)

[24] Österle W, Prietzel C, Kloß H, Dmitriev A I. On the role of copper in brake friction materials. *Tribol Int* **43**(12): 2317–2326 (2010)

[25] Kukutschová J, Moravec P, Tomášek V, Matějka V, Smolík J, Schwarz J, Seidlerová J, Šafářová K, Filip P. On airborne nano/micro-sized wear particles released from low-metallic automotive brakes. *Environ Pollut* **159**(4): 998–1006 (2011)

[26] Lee P W, Filip P. Friction and wear of Cu-free and Sb-free environmental friendly automotive brake materials. *Wear* **302**(1–2): 1404–1413 (2013)

[27] Belhocine A, Omar W Z W. Predictive modeling and simulation of the structural contact problems between the brake pads and rotor in frictional sliding contact. *Int J Interact Des Manuf Ijidem* **12**(1): 63–80 (2018)

[28] Stoica N A, Petrescu A M, Tudor A. Modelling the wear processes of the automotive brake pad and disc. *INCAS BULLETIN* **10**(4): 169–179 (2018)

[29] Ogbeide S O, Anwule P D. Modelling of automobile brake pad wear. *Iconic Res Eng J* **3**(4) : 227–239 (2019).

[30] Riva G, Perricone G, Wahlström J. A multi-scale simulation approach to investigate local contact temperatures for commercial Cu-full and Cu-free brake pads. *Lubricants* **7**(9): 80 (2019)

[31] Sawczuk W, Merkisz-Guranowska A, Ulbrich D, Kowalczyk J, Cañás A M R. Investigation and modelling of the weight wear of friction pads of a railway disc brake. *Materials* **15**(18): 6312 (2022)

[32] Gurumoorthy S, Bourgeau A, Bhumireddy Y, Allipur S R, Sridhar S. Tribological behaviour of an automotive brake pad system under Los Angeles city traffic test conditions. *SAE Int J Adv & Curr Prac Mobility* **4**(6): 2235–2241 (2022)

[33] Ricciardi V, Augsburg K, Gramstat S, Schreiber V, Ivanov V. Survey on modelling and techniques for friction estimation in automotive brakes. *Appl Sci* **7**(9): 873 (2017)

[34] Ricciardi V, Travagliati A, Schreiber V, Klomp M, Ivanov V, Augsburg K, Faria C. A novel semi-empirical dynamic brake model for automotive applications. *Tribol Int* **146**: 106223 (2020)

[35] Riva G, Varriale F, Wahlström J. A finite element analysis (FEA) approach to simulate the coefficient of friction of a brake system starting from material friction characterization. *Friction* **9**(1): 191–200 (2021)

[36] Federici M, Perricone G, Gialanella S, Straffelini G. Sliding behaviour of friction material against cermet coatings: Pin-on-disc study of the running-in stage. *Tribol Lett* **66**(2): 53 (2018)

[37] Edmundson H P. *Theory of Self Reproducing Automata*. Urbana (USA): University of Illinois Press, 1966.

[38] Müller M, Ostermeyer G P. A cellular automaton model to describe the three-dimensional friction and wear mechanism of brake systems. *Wear* **263**(7–12): 1175–1188 (2007)

[39] Mueller M, Ostermeyer G P. Cellular automata method for macroscopic surface and friction dynamics in brake systems. *Tribol Int* **40**(6): 942–952 (2007)

[40] Wahlström J, Söderberg A, Olofsson U. A cellular automaton approach to numerically simulate the contact situation in disc brakes. *Tribol Lett* **42**(3): 253–262 (2011)

[41] Wahlström J. Towards a cellular automaton to simulate friction, wear, and particle emission of disc brakes. *Wear* **313**(1–2): 75–82 (2014)

[42] Ostermeyer G P, Merlis J H. Modeling the friction boundary layer of an entire brake pad with an abstract cellular automaton. *Lubricants* **6**(2): 44 (2018)

[43] Federici M, Alemani M, Menapace C, Gialanella S, Perricone G, Straffelini G. A critical comparison of dynamometer data with pin-on-disc data for the same two friction material pairs—A case study. *Wear* **424–425**: 40–47 (2019)

[44] Archard J F. Contact and rubbing of flat surfaces. *J Appl Phys* **24**(8): 981–988 (1953)

[45] Archard J F. Friction between metal surfaces. *Wear* **113**(1): 3–16 (1986)

[46] Kopf P W. Phenolic resins. In *Encyclopedia of Polymer Science and Technology*, Mark H F, Ed. Hoboken (USA): John Wiley & Sons, Inc. 2002: 1–54.

[47] Muc A, Romanowicz P, Chwał M. Description of the resin curing process—Formulation and optimization. *Polymers* **11**(1): 127 (2019)

[48] D. A. S. Razo and D. Pellerej. Control of gaseous emission during the curing of novolac phenolic resin in friction materials production. *SAE International Journal of Materials and Manufacturing* **7**(1): 10–16 (2014)

[49] Gurunath P V, Bijwe J. Potential exploration of novel green resins as binders for NAO friction composites in severe operating conditions. *Wear* **267**(5–8): 789–796 (2009)

[50] Straffelini G. *Friction and Wear—Methodologies for Design and Control*. New York (USA): Springer Cham, 2015

[51] Straffelini G, Gialanella S. Airborne particulate matter from brake systems: An assessment of the relevant tribological formation mechanisms. *Wear* **478–479**: 203883 (2021)

[52] Eriksson M, Bergman F, Jacobson S. On the nature of tribological contact in automotive brakes. *Wear* **252**(1–2): 26–36 (2002)

[53] Jayashree P, Candeo S, Matějka V, Foniok K, Leonardi M, Straffelini G. Study on the effect of the addition of bulk and exfoliated graphitic carbon nitride on the dry sliding behavior of a commercial friction material formulation through pin on disc and subscale dynamometer analysis. *Tribol Int* **179**: 108152 (2023)

[54] Şirin Ş, Akıncıoğlu S, Gupta M K, Kıvak T, Khanna N. A tribological performance of vegetable-based oil combined with GNPs and hBN nanoparticles on the friction-wear tests of titanium grade 2. *Tribol Int* **181**: 108314 (2023)

[55] Shen M X, Li H X, Du J H, Ji D H, Liu S P, Xiao Y L. New insights into reducing airborne particle emissions from brake materials: Grooved textures on brake disc surface. *Tribol Int* **174**: 107721 (2022)

[56] Rabinowicz E. *Friction and Wear of Materials*. New York (USA): John Wiley and Sons, 1965.

[57] Jiang J R, Stott F H, Stack M M. The role of triboparticulates in dry sliding wear. *Tribol Int* **31**(5): 245–256 (1998)

[58] Stott F H. The role of oxidation in the wear of alloys. *Tribol Int* **31**(1–3): 61–71 (1998)

[59] Abenojar J, del Real J C, Martinez M A, de Santayana M C. Effect of silane treatment on SiC particles used as reinforcement in epoxy resins. *J Adhes* **85**(6): 287–301 (2009)

[60] Scharf T W, Prasad S V. Solid lubricants: A review. *J Mater Sci* **48**(2): 511–531 (2013)

[61] Dante R C. (2016) Tribology of friction materials. In *Handbook of Friction Materials and their Applications*. Amsterdam: Elsevier, 2016: 7–28.

[62] Österle W, Griepentrog M, Gross T, Urban I. Chemical and microstructural changes induced by friction and wear of brakes. *Wear* **251**(1–12): 1469–1476 (2001)

[63] Neis P D, Ferreira N F, Fekete G, Matozo L T, Masotti D. Towards a better understanding of the structures existing on the surface of brake pads. *Tribol Int* **105**: 135–147 (2017)

[64] Ostermeyer G P, Müller M. Dynamic interaction of friction and surface topography in brake systems. *Tribol Int* **39**(5): 370–380 (2006)

Davide CARLEVARIS. He acquired a background in energy, environment, and sustainable development at the University of Trento, Italy, where he received his master degree in materials and production engineering. He is currently undertaking doctoral research there in the field of automotive brake systems. In collaboration with Brembo University, USA and Lund University, Sweden, his work mainly focuses on the sustainability aspect of brake pads.

Francesco VARRIALE. He received his master degree in mechanical engineering in 2014 from Naples University, Italy. After that, he joined Brembo N.V. in the R&D department and started his Ph.D. in mechanical engineering at Faculty of Engineering (LTH), Lund University, Sweden, in 2020 as an industrial student. His research is focused on brake friction and emissions and on the development of innovative simulation methodologies.

Jens WAHLSTRÖM. He held the Professor Chair in machine elements at Faculty of Engineering, Lund University, Sweden, 2019. His research focuses on the tribological performance and non-exhaust emissions of machine elements in road and rail vehicles. He employs both experimental and simulation methods in his work. Dr. Wahlström actively participates in several international interdisciplinary research projects.

Cinzia MENAPACE. She graduated in materials engineering at the University of Trento, Italy, in 1999. She received her Ph.D. degree in metallurgical engineering from the University of Padova, Italy, in 2003. She has been working as a junior and senior researcher at the University of Trento, Italy, for 20 years. Her current position is an associate professor of Metallurgy at University of Trento, Italy. Her research interests include powder metallurgy, friction materials, and hot workability of metals.